Research Article | Vol. 28, No. 3 / 3 February 2020 / Optics Express 3280
Optics EXPRESS

Tunable narrow-linewidth laser at 2 μm wavelength for gravitational wave detector research

D. P. KAPASI,[1,*] J. EICHHOLZ,[1] T. MCRAE,[1] R. L. WARD,[1] B. J. J. SLAGMOLEN,[1] S. LEGGE,[2] K. S. HARDMAN,[2] P. A. ALTIN,[1] AND D. E. MCCLELLAND[1]

[1] *OzGrav, Centre for Gravitational Astrophysics, Department of Quantum Science, Research School of Physics, Australian National University, Acton, ACT 2601, Australia*
[2] *Quantum Sensors Group, Department of Quantum Science, Research School of Physics, Australian National University, Acton, ACT 2601, Australia*
[*] *disha.kapasi@anu.edu.au*

Abstract: We present and characterize a narrow-linewidth external-cavity diode laser at 2 μm, and show that it represents a low-cost, high-performance alternative to fiber lasers for research into 2 μm photonic technologies for next-generation gravitational-wave detectors. A linewidth of 20 kHz for a 10 ms integration time was measured without any active stabilization, with frequency noise of $\sim 15\ \mathrm{Hz}/\sqrt{\mathrm{Hz}}$ between 3 kHz and 100 kHz. This performance is suitable for the generation of quantum squeezed light, and we measure intensity noise comparable to that of master oscillators used in current gravitational wave interferometers. The laser wavelength is tunable over a 120 nm range, and both the frequency and intensity can be modulated at up to 10 MHz by modulating the diode current. These features also make it suitable for other emerging applications in the 2 μm wavelength region including gas sensing, optical communications and LIDAR.

1. Introduction

The first direct detection of gravitational waves (GW) in 2015 by the Advanced Laser Interferometer Gravitational-Wave Observatory (aLIGO) came from a pair of black holes 1.3 billion light years away [1]. This marked the beginning of the era of GW astronomy, with nearly a dozen binary inspiral detections by the ground-based observatories LIGO and Virgo in their first two coordinated observation runs [2,3]. Increasing the event rates and signal-to-noise ratios for future observations requires improving the individual detector sensitivities, which are generally limited by a combination of classical and quantum-mechanical noise sources. An enhanced detector performance will extend the horizon for GW observations, enable black-hole spectroscopy, inform models for the neutron star equation of state [4] and allow the observation of coalescences from Population III stars with larger redshifts [5]. To overcome the current limitations it is necessary to not only understand and mitigate the principal noise sources, but also test new technologies that promise to improve the sensitivity of current and future GW detectors.

Next-generation interferometric GW observatories will likely operate with silicon test masses at cryogenic temperatures to reduce the impact of thermal noise in mirror coatings and substrates. The transition away from fused silica will require the operating wavelength to shift from 1 μm to the 1.55 – 2 μm region. Being a primary telecommunication wavelength, 1.55 μm is more technologically developed, but there are advantages in choosing longer wavelengths: intra-substrate and coating absorption reduces and the amount of optical scatter due to the residual micro-roughness of the optics scales as $1/\lambda^2$ [6,7].

#383685 https://doi.org/10.1364/OE.383685
Journal © 2020 Received 25 Nov 2019; revised 12 Jan 2020; accepted 13 Jan 2020; published 23 Jan 2020

Optics EXPRESS

Operating the detector at longer wavelengths has many challenges – developing lasers, photodiodes with high quantum efficiency [8], low-mechanical-loss optical coatings [9,10] and the generation of quantum squeezed light [11–14] – which are areas of active research. However, this research is currently hindered by the availability and expense of 2 μm photonic technology. While high-power fiber lasers suitable for use as the main interferometer beam are under development [15], there is a pressing need for a low-cost, low-noise 2 μm laser source with a narrow linewidth to accelerate research in adjacent areas, including squeezed light generation [11,13].

In recent decades, semiconductor diode lasers have revolutionized the fields of spectroscopy, atomic physics and quantum optics, and the range of wavelengths which they cover is continually expanding. External cavity diode lasers (ECDLs) provide single spectral and spatial mode operation with narrow linewidth, wide tuning range and high-speed modulation capabilities, all at relatively low cost compared to other laser types. ECDLs typically operate in Littman-Metcalf [16] or Littrow [17,18] configurations where a dispersive element is used to selectively provide optical feedback.

Here we present an ECDL operating in the 2 μm wavelength range, and characterize its performance and tunability. The development of a simple and inexpensive low power 2 μm laser will accelerate research efforts on other 2 μm technologies. In addition to enabling next-generation GW detector research, this laser may also find applications in medicine, gas sensing, remote sensing, precision metrology, optical telecommunications, defense and LIDAR [19–22].

2. ECDL design and experimental setup

Our ECDL design is centered around a commercial single-angled-facet (SAF) gain module with a center wavelength of 1920 nm (Thorlabs SAF1900S), used in Littrow configuration (Fig. 1(a)). The SAF design uses a curved ridge waveguide such that the output beam exits the front facet at an angle, suppressing backreflections which would cause unwanted feedback into the gain medium. The module has a single-mode fiber coupled to the normal facet of the chip and an integrated thermistor and thermo-electric cooler for temperature control. Similar modules have been used in ECDLs operating at 1 μm [23] and 1.55 μm [24]; our design is adapted from [24].

Light exits the free-space output of the gain chip at an angle of 26.5° and a full width at half maximum (FWHM) lateral divergence angle of 19°, which we collimate using a molded IR aspheric lens (Thorlabs 390093-D) with a numerical aperture (NA) of 0.71 and an effective focal length of 3 mm. The lens is held in a custom mount which provides fine adjustment along the optical axis using push-pull screws.

The external cavity is formed by a blazed reflective diffraction grating with a ruling of 600 lines/mm (Thorlabs GR13-0616) and ~90% first-order diffraction efficiency for p polarization at 2 μm. The dispersion coefficient of the grating is 1.46 nm/mrad. The grating is held in a high-stability kinematic mount with an integrated piezo-electric (PZT) drive (Thorlabs Polaris-K1P). The length of the external cavity is approximately $L_{EC} = 20$ mm which results in a free spectral range of $FSR_{EC} = c/2L_{EC} \sim 7.5$ GHz. An external fiber-coupled, polarization-insensitive optical isolator with an insertion loss of 1 dB and 30 dB isolation was spliced to the fiber output of the ECDL to protect it from back-reflected light. The entire assembly is housed in a monolithic aluminium enclosure and placed in an acoustically insulated box vibrationally isolated from the table via viscoelastic dampers.

To characterize the performance of the ECDL, a thermally-isolated unbalanced fiber Mach-Zehnder interferometer (fMZI) was used as a frequency reference (Fig. 1(c)). The fMZI has a path-length mismatch of approximately 10 m, resulting in a fringe spacing of 18 MHz at 2 μm. To counteract differential drift between the laser frequency and the fMZI, predominantly caused by temperature variations in the lab, a low-bandwidth (unity-gain frequency < 10 Hz) servo loop feeding back to the grating PZT was used to keep the fMZI output in its mid-fringe linear

Optics EXPRESS

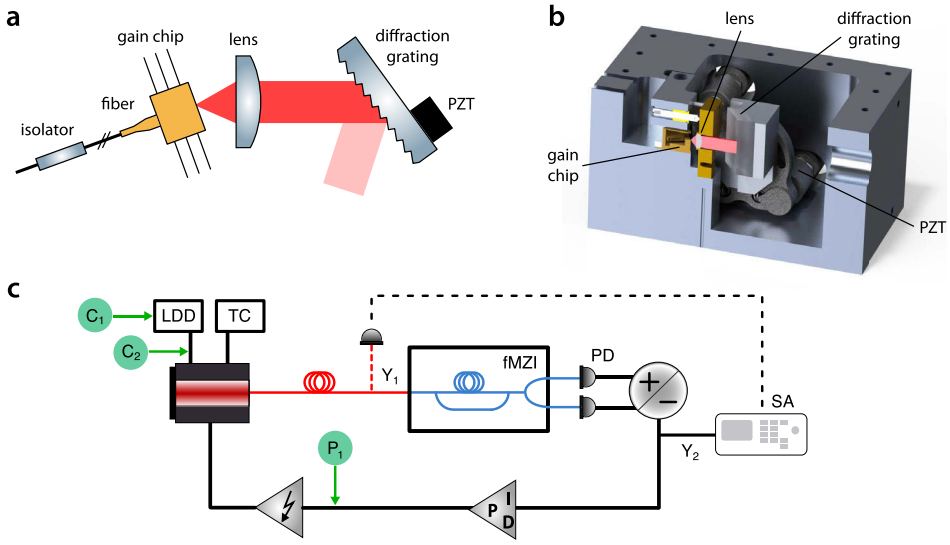

Fig. 1. (a, b) Schematic and design of the 2 μm ECDL. (c) Experimental setup for characterization: LDD - laser diode current driver, TC - temperature controller, fMZI - fiber Mach-Zehnder interferometer with 10 m delay line, SA - spectrum analyzer, PD - photodetector. C_1 and C_2 are injection points for current modulation, P_1 is the injection point for PZT modulation. Intensity noise and modulation are measured at Y_1, while frequency noise and modulation are measured at the fMZI output Y_2.

operating range. The diode current and temperature were controlled using commercial driver units (Newport 505B, ILX Lightwave LDT-5412).

3. Characterization of the ECDL

3.1. Output power and tuning range

The measured optical power exiting the fiber after the isolator is presented in Fig. 2(a) as a function of injection current. From this measurement, the threshold current was determined to be 109±1 mA and the output efficiency was 25.4±1 μW/mA. The maximum measured optical power was 9.3 mW at 480 mA, limited by the current driver. The SAF gain chip has a maximum operating current of 800 mA, which should allow an output power of up to 17.5 mW. For the

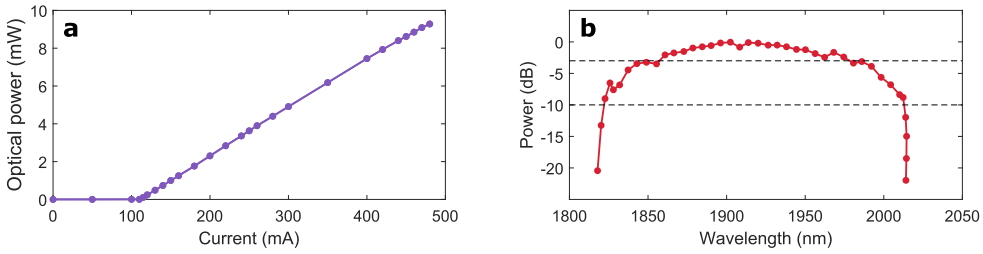

Fig. 2. (a) Measured optical output power (after the isolator) as a function of injection current into the ECDL at 1920 nm. (b) Coarse wavelength tuning range with an injection current of 400 mA. The FWHM (-3 dB) tuning range is 120 nm.

Optics EXPRESS

measurements described below, the diode was operated at 400 mA with approximately 7.5 mW of optical power after the isolator. Single-mode operation was verified by injecting the output beam into a bowtie cavity with a length of 46 cm and a linewidth of 16.5 MHz at 2 μm.

The coarse tuning range (not mode-hop-free) of the ECDL was measured by tuning the angle of the diffraction grating which forms one end of the external cavity. The measurement was calibrated against a 1984 nm thulium (Tm) fiber laser (AdValue Photonics). The output power as a function of wavelength is shown in Fig. 2(b) for an injection current of 400 mA. The ECDL has a FWHM (-3 dB) and full width at one-tenth of maximum (FWTM, -10 dB) tuning range of 120±5 nm and 190±5 nm respectively around a center wavelength of approximately 1920 nm. The FWHM decreased by approximately 25% with a lower injection current of 200 mA. The typical mode-hop-free tuning range of the ECDL was ~ 5 GHz without feedforward to the injection current.

3.2. Intensity noise

We attempted to measure the relative intensity noise (RIN) of the ECDL using a single extended InGaAs photodetector (Thorlabs PDA10D2) placed at the output of the fiber (point Y_1 in Fig. 1(c)). This measurement is shown in Fig. 3 as a function of frequency between 1 Hz and 100 kHz. The measurement is limited by the $1/\sqrt{f}$ dark noise of the photodetector, and thus provides only an upper bound on the RIN of the ECDL. This upper bound is approximately 2×10^{-7} at 100 Hz, falling to 5×10^{-8} at 10 kHz. The dashed line on the plot indicates the expected shot noise of the ECDL which has a level of 2.5×10^{-8} Hz$^{-1/2}$. For comparison, the RIN of a commercial Tm fiber laser measured using the same setup is also shown. The fact that we cannot measure the true RIN of the ECDL due to the dark noise of the photodetector highlights the need for further development of 2 μm photonic technologies. The performance measured here is comparable to the 1064 nm non-planar ring oscillators (NPRO) used as the master laser in current-generation GW observatories [25].

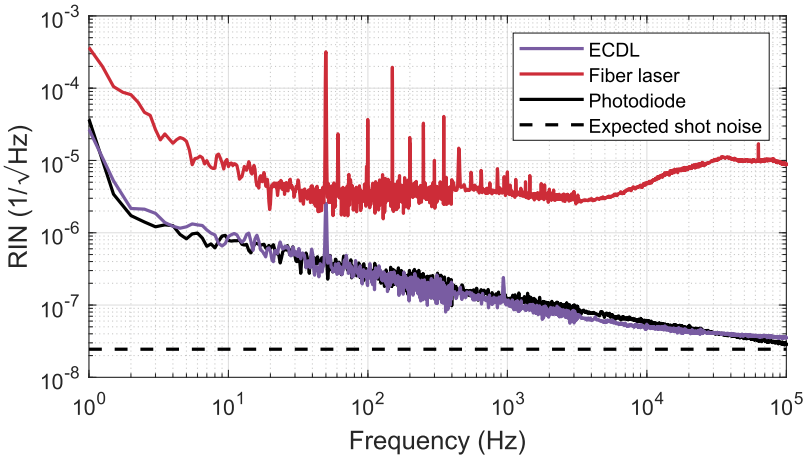

Fig. 3. Relative intensity noise (RIN) of the ECDL (lavender) and commercial Tm fiber laser (red). The ECDL measurement is limited by photodiode dark noise across the entire range, and thus provides only an upper bound on the RIN of the ECDL.

3.3. Frequency noise

The frequency noise of the ECDL was measured against the fringes of the fMZI that is illustrated in Fig. 1(c). The fMZI is operated at mid-fringe. Its relatively short 10 m length mismatch causes

Optics EXPRESS

a high degree of correlation between the two paths upon their recombination, allowing us to attribute the observed differential phase fluctuations $\delta\phi$ to frequency shifts $\delta\nu = \frac{18\,\mathrm{MHz}}{2\pi}\delta\phi$ of the laser. The voltage noise spectra measured at the output photodetectors (Thorlabs PDA10D2) carry the combined signatures of intensity and frequency noise. However, the intensity noise registered by both has positive correlation, while the frequency noise is anti-correlated. This allows us to electronically equalize the signal levels and synthesize a balanced homodyne readout, whose differential channel isolates frequency noise and rejects intensity noise by 45 dB. The frequency noise spectra shown in Fig. 4 were recorded using an FFT spectrum analyzer with a 100 kHz span. The baseline level of photodetector dark and amplifier noise, scaled to frequency noise units by the slope of the fMZI response to the ECDL input, is shown in black.

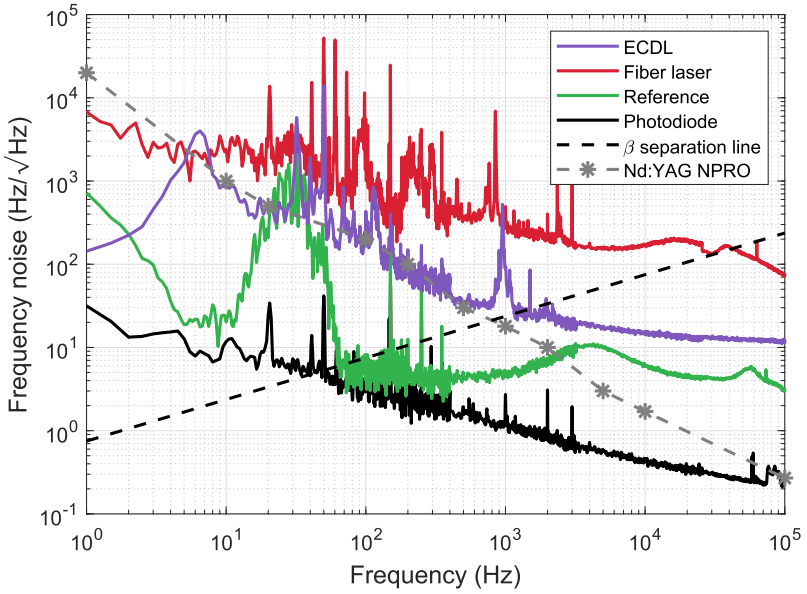

Fig. 4. Frequency noise of ECDL (lavender) compared to the Tm fiber laser (red) and a 1.55 μm reference (green). The dashed line is the β separation line (description in text). The roll-off of the ECDL noise below 10 Hz is due to the suppression of the feedback loop used to counteract thermal drift. The reference laser did not require this feedback, which is why the green trace continues to rise below 10 Hz.

We report nearly flat frequency noise from a level of 20 Hz/$\sqrt{\text{Hz}}$ at 3 kHz to 12 Hz/$\sqrt{\text{Hz}}$ at 100 kHz. Above 200 Hz, the frequency noise of the ECDL is lower than that of the commercial Tm fiber laser, by up to an order of magnitude at frequencies around 10 kHz [26]. Figure 4 also shows the typical frequency noise spectrum of a 1.064 μm Nd:YAG NPRO laser [27]. The 2 μm ECDL performance is comparable below 1 kHz, although at frequencies above this the ECDL noise flattens out while the NPRO noise continues to fall as $1/f$.

One disadvantage of the method used here is that it cannot distinguish between laser frequency noise and phase fluctuations in the fMZI. The fMZI must therefore be well isolated to protect it from environmental noise sources, which tend to increase at low frequencies. Alternative techniques such as the delayed self-heterodyne interferometry (DSHI) method [24,28,29] get around this by shifting the frequency of one of the arms and delaying it beyond the coherence time of the laser, so that the recombined beams are entirely uncorrelated. However, high-speed modulators and, for narrow linewidth lasers, multiple kilometers of fiber are required to satisfy this condition. Affordable fiber types that would allow such long optical delay lines generally exhibit too high attenuation at 2 μm to make this approach feasible for our investigation.

Optics EXPRESS

Here, we instead verified experimentally that phase fluctuations of the fMZI do not limit our measurement using a commercial narrow-linewidth 1.55 μm fiber laser (Koheras Basik X15) as an additional low-noise frequency reference. To ensure that this measurement could be used as a valid reference, the same fibers and photodetectors were used. The reference trace in Fig. 4 is a combination of the frequency noise of this reference laser and environmental noise in the fMZI; the two cannot be distinguished in this setup. The margin between the reference trace and the ECDL frequency noise indicates that our measurement is not intrinsically limited by phase noise in the fMZI. There is a small region around 20 – 50 Hz where the green trace rises above the ECDL noise, which could be due to environmental noise affecting the reference laser. The peak at 1 kHz in the ECDL trace can be attributed to a mechanical resonance in the laser mount.

3.4. Linewidth

Although a measurement of frequency noise such as that presented in Fig. 4 contains complete information about the frequency stability of a laser, it is often useful to summarize this information in a single linewidth value at some specified integration time. The lineshape of a laser in general can be viewed as a Voigt profile with contributions from both Gaussian and Lorentzian components. For an ECDL, the Gaussian linewidth originates from environmental sources and is not power dependent, whereas the Lorentzian linewidth arises from spontaneous emission and is inversely proportional to the optical power [30]. It is possible to derive the lineshape numerically from the frequency noise spectrum [31], but the process is not straightforward. Here we use a simple method for estimating the Gaussian linewidth from the frequency noise spectrum, first described in [32]. Frequency noise can be interpreted in terms of a modulation index β, where β is the ratio of the frequency noise level to its Fourier frequency. The width of the Gaussian lineshape is the sum of contributions from high-modulation-index noise components [32], those which lie above the so-called β-separation line given by $8\ \ln(2) f/\pi^2$ (dashed line in Fig. 4). Noise below this line contributes primarily to the Lorentzian wings of the lineshape but does not affect the linewidth. For our ECDL, integrating above the β-separation line from 100 Hz results in a 10-ms-integration-time FWHM Gaussian linewidth of 19.5 kHz. Integrating above 1 kHz for the 1 ms integration time gives a linewidth of 2 kHz. For comparison, the commercial Tm fiber laser (red trace in Fig. 4) has a Gaussian linewidth of 36 kHz for a 1 ms integration time. The linewidth of the ECDL is dominated by the mechanical resonance at 1 kHz, which could potentially be eliminated with a different external cavity design such as that used in [23].

3.5. Modulation

The ability to modulate the intensity and frequency of a laser is important for many applications, particularly for frequency stabilization and linewidth narrowing. Semiconductor diode lasers typically have very high modulation bandwidths into the gigahertz regime when the diode injection current is modulated directly [33]. In addition, the frequency of an ECDL can be modulated in the same way that wavelength tuning is achieved; in our case, by changing the angle of the diffraction grating using the piezo-electric transducer (PZT).

Figure 5 shows the modulation characteristics of our ECDL for both current and PZT input. The current modulation signal was injected into the current driver (point C_1 in Fig. 1(c)) for frequencies below 100 kHz, and via a bias-tee (point C_2) for higher frequencies. The PZT modulation signal was injected before the high-voltage amplifier (P_1 in Fig. 1(c)). The resulting intensity and frequency modulations were measured in the same way as the intensity and frequency noise at points Y_1 and Y_2. The modulation transfer functions were recorded as a function of frequency between 10 Hz and 25 MHz using a frequency response analyzer (Liquid Instruments Moku:Lab).

The current modulation response of the ECDL is approximately flat in both intensity and frequency and displays no noteworthy features below 1 MHz. The intensity modulation bandwidth

Optics EXPRESS

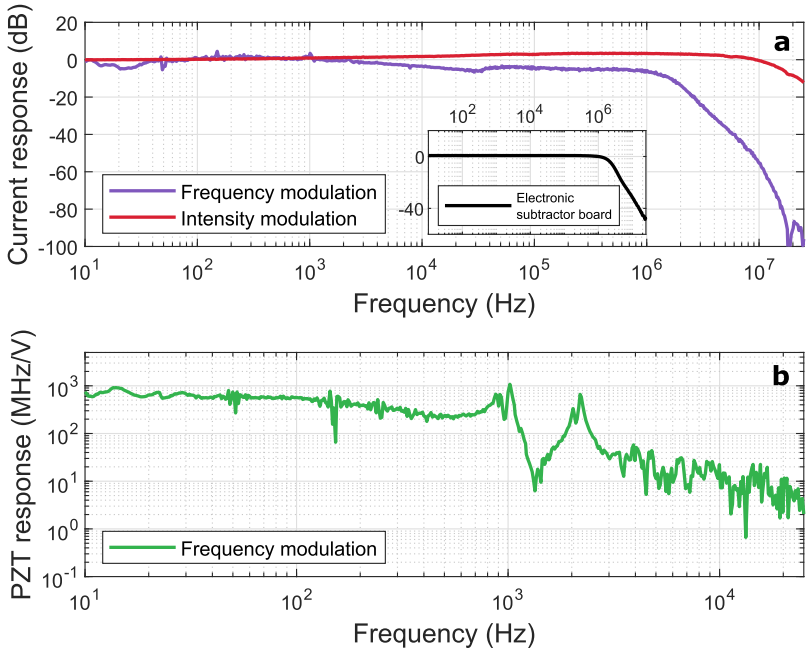

Fig. 5. Modulation response of the ECDL. (a) Frequency and intensity response to current modulation. The 0 dB level corresponds to 35 MHz/mA in frequency and 25 μW/mA in intensity. Inset shows the response of the electronic subtractor board which rolls off at 1 MHz. (b) Frequency response to PZT modulation. Mechanical resonances are visible at 1 kHz and 2 kHz.

is at least 15 MHz, with our measurement being limited by the bandwidth of the photodetector. The frequency modulation measurement is limited additionally by the bandwidth of the electronic subtractor used to derive the balanced homodyne readout, but is flat up to at least 1 MHz. The current modulation amplitude within the passband is 25 μW/mA in intensity and 35 MHz/mA in frequency.

The PZT modulation response displays resonances at 1 kHz and 2 kHz, likely due to mechanical resonances in the lens or grating mount. Below this frequency, the response is flat at approximately 560 MHz/V (112 MHz/μrad), in agreement with the tuning coefficient determined from the dispersion coefficient of the grating. For comparison, the typical mode-hop-free tuning range of the laser is approximately 5 GHz. The usable bandwidth of the PZT is therefore limited to approximately 1 kHz, although this could be improved with a different mechanical design for the lens or grating mount [23]. The relative intensity modulation caused by the PZT was measured to be no larger than 0.1%/V, which corresponds to an AM-FM coupling of approximately 0.2%/GHz.

4. Conclusion

We have constructed a 2-μm-band ECDL with over 9 mW of usable output power and a broad 120 nm tuning range from low-cost commercial components. The laser exhibits nearly flat frequency noise at around 15 Hz/$\sqrt{\text{Hz}}$ from 3 kHz to 100 kHz, and its 10 ms Gaussian linewidth is 20 kHz, making it a viable seed for precision interferometric experiments. With higher diode current, the output power may be increased to above 15 mW. The ECDL is frequency-tunable with high bandwidth via modulation of the diode current, PZT-based actuation of the grating angle, and temperature control of the gain chip. The high grating dispersion gives the piezo-tuning a large response of 560 MHz/V, enabling fast ramping of the laser wavelength for scanning applications.

Optics EXPRESS

This simple and robust ECDL will enable development of 2 μm photonic technologies, and has potential to be used as the seed laser for squeezed light generation in future gravitational wave detectors.

Funding

Australian Research Council (CE170100004).

Acknowledgments

The authors would like to thank R. Adhikari, N. Robins, P. Wigley and C. Freier for valuable discussions.

References

1. LIGO Scientific Collaboration and Virgo Collaboration, "Observation of gravitational waves from a binary black hole merger," Phys. Rev. Lett. **116**(6), 061102 (2016).
2. LIGO Scientific Collaboration and Virgo Collaboration, "GWTC-1: A gravitational-wave transient catalog of compact binary mergers observed by LIGO and Virgo during the first and second observing runs," Phys. Rev. X **9**(3), 031040 (2019).
3. LIGO Scientific Collaboration and Virgo Collaboration, "Binary black hole population properties inferred from the first and second observing runs of advanced LIGO and advanced Virgo," Astrophys. J., Lett. **882**(2), L24 (2019).
4. M. Agathos, J. Meidam, W. Del Pozzo, T. G. F. Li, M. Tompitak, J. Veitch, S. Vitale, and C. Van Den Broeck, "Constraining the neutron star equation of state with gravitational wave signals from coalescing binary neutron stars," Phys. Rev. D **92**(2), 023012 (2015).
5. E. Berti, A. Sesana, E. Barausse, V. Cardoso, and K. Belczynski, "Spectroscopy of Kerr black holes with earth and space-based interferometers," Phys. Rev. Lett. **117**(10), 101102 (2016).
6. S. Rowan, R. L. Byer, M. M. Fejer, R. K. Route, G. Cagnoli, D. R. Crooks, J. Hough, P. H. Sneddon, and W. Winkler, "Test mass materials for a new generation of gravitational wave detectors," in *Gravitational-Wave Detection*, vol. 4856 P. Saulson and A. M. Cruise, eds., International Society for Optics and Photonics (SPIE, 2003), pp. 292–297.
7. J. Steinlechner, I. W. Martin, A. S. Bell, J. Hough, M. Fletcher, P. G. Murray, R. Robie, S. Rowan, and R. Schnabel, "Silicon-based optical mirror coatings for ultrahigh precision metrology and sensing," Phys. Rev. Lett. **120**(26), 263602 (2018).
8. P. Martyniuk, J. Antoszewski, M. Martyniuk, L. Faraone, and A. Rogalski, "New concepts in infrared photodetector designs," Appl. Phys. Rev. **1**(4), 041102 (2014).
9. The LIGO Scientific Collaboration, LIGO Voyager upgrade design concept, LIGO Technical Note No. T1400226 (2019).
10. The LIGO Scientific Collaboration, Instrument science white paper, LIGO Technical Note No. T1900409 (2019).
11. G. L. Mansell, T. G. McRae, P. A. Altin, M. J. Yap, R. L. Ward, B. J. J. Slagmolen, D. A. Shaddock, and D. E. McClelland, "Observation of squeezed light in the 2 μm region," Phys. Rev. Lett. **120**(20), 203603 (2018).
12. M. J. Yap, D. W. Gould, T. G. McRae, P. A. Altin, N. Kijbunchoo, G. L. Mansell, R. L. Ward, D. A. Shaddock, B. J. J. Slagmolen, and D. E. McClelland, "Squeezed vacuum phase control at 2 μm," Opt. Lett. **44**(21), 5386 (2019).
13. The LIGO Scientific Collaboration, "Quantum-Enhanced Advanced LIGO Detectors in the Era of Gravitational-Wave Astronomy," Phys. Rev. Lett. **123**(23), 231107 (2019).
14. Collaboration Virgo, "Increasing the Astrophysical Reach of the Advanced Virgo Detector via the Application of Squeezed Vacuum States of Light," Phys. Rev. Lett. **123**(23), 231108 (2019).
15. N. Simakov, A. V. Hemming, A. Carter, K. Farley, A. Davidson, N. Carmody, M. Hughes, J. M. O. Daniel, L. Corena, D. Stepanov, and J. Haub, "Design and experimental demonstration of a large pedestal thulium-doped fibre," Opt. Express **23**(3), 3126 (2015).
16. Sang Eon Park, Yong Kwon Taeg, Shin Eun-Joo, and Seong Lee Ho, "A compact extended-cavity diode laser with a Littman configuration," IEEE Trans. Instrum. Meas. **52**(2), 280–283 (2003).
17. L. Ricci, M. Weidemüller, T. Esslinger, A. Hemmerich, C. Zimmermann, V. Vuletic, W. König, and T. Hänsch, "A compact grating-stabilized diode laser system for atomic physics," Opt. Commun. **117**(5-6), 541–549 (1995).
18. K. B. MacAdam, A. Steinbach, and C. Wieman, "A narrow-band tunable diode laser system with grating feedback, and a saturated absorption spectrometer for Cs and Rb," Am. J. Phys. **60**(12), 1098–1111 (1992).
19. B. Pal, "Frontiers in guided wave optics and optoelectronics," in *Frontiers in Guided Wave Optics and Optoelectronics*, B. Pal, ed. (IntechOpen, 2010), Chap. 1.
20. J. Geng, Q. Wang, and S. Jiang, "2 μm fiber laser sources and their applications," in *Nanophotonics and Macrophotonics for Space Environments V*, vol. 8164 E. W. Taylor and D. A. Cardimona, eds., International Society for Optics and Photonics (SPIE, 2011), pp. 79–88.
21. K. Scholle, S. Lamrini, P. Koopmann, and P. Fuhrberg, "2 μm laser sources and their possible applications," in *Frontiers in Guided Wave Optics and Optoelectronics*, B. Pal, ed. (IntechOpen, 2010), Chap. 22.

Optics EXPRESS

22. A. Hemming, N. Simakov, J. Haub, and A. Carter, "A review of recent progress in holmium-doped silica fibre sources," Opt. Fiber Technol. **20**(6), 621–630 (2014).
23. D. K. Shin, B. M. Henson, R. I. Khakimov, J. A. Ross, C. J. Dedman, S. S. Hodgman, K. G. H. Baldwin, and A. G. Truscott, "Widely tunable, narrow linewidth external-cavity gain chip laser for spectroscopy between 1.0 - 1.1 μm," Opt. Express **24**(24), 27403 (2016).
24. S. Bennetts, G. D. McDonald, K. S. Hardman, J. E. Debs, C. C. N. Kuhn, J. D. Close, and N. P. Robins, "External cavity diode lasers with 5 kHz linewidth and 200 nm tuning range at 1.55 μm and methods for linewidth measurement," Opt. Express **22**(9), 10642 (2014).
25. "Mephisto Applications in Gravitational Waves Detection," Coherent white paper, 2016 (www.coherent.com).
26. G. L. Mansell, "Squeezed light sources for current and future interferometric gravitational-wave detectors," Ph.D. thesis (Australian National University, 2018.
27. P. Kwee and B. Willke, "Automatic laser beam characterization of monolithic Nd:YAG nonplanar ring lasers," Appl. Opt. **47**(32), 6022 (2008).
28. T. Okoshi, K. Kikuchi, and A. Nakayama, "Novel method for high resolution measurement of laser output spectrum," Electron. Lett. **16**(16), 630 (1980).
29. L. Richter, H. Mandelberg, M. Kruger, and P. McGrath, "Linewidth determination from self-heterodyne measurements with subcoherence delay times," IEEE J. Quantum Electron. **22**(11), 2070–2074 (1986).
30. K. Kikuchi and T. Okoshi, "Dependence of semiconductor laser linewidth on measurement time: evidence of predominance of 1/f noise," Electron. Lett. **21**(22), 1011 (1985).
31. D. S. Elliott, R. Roy, and S. J. Smith, "Extracavity laser band shape and bandwidth modification," Phys. Rev. A **26**(1), 12–18 (1982).
32. G. D. Domenico, S. Schilt, and P. Thomann, "Simple approach to the relation between laser frequency noise and laser line shape," Appl. Opt. **49**(25), 4801 (2010).
33. C. E. Wieman and L. Hollberg, "Using diode lasers for atomic physics," Rev. Sci. Instrum. **62**(1), 1–20 (1991).